ISSN (Online) 2395-2717

International Journal of Engineering Research in Electrical and Electronic Engineering (IJEREEE)

Vol 10, Issue 1, January 2023

Miniaturization, Characterization and X-Ray Diffraction Peak Analization of Magnetic Nanoparticles

[1] Mahendra D. Shelar*, [2] C.T. Birajdar, [3] Sudarshana G. Badhe, [4] V.A. Shelke, [5] B.H. Devmunde

[1] Department of Chemistry, Rajarshi Shahu Art's, Commerce and Science College, Pathri, Maharashtra, India
[2] Department of Physics, Shri Madhavrao Patil Mahavdyalaya, Murum, Omerga, Osmanabad, India
[3] Department of Physics, R.B. Attal Arts, Science and Commerce College, Georai, Beed, Maharashtra, India
[4] Department of Chemistry, Indraraj Arts,Commerce and Science College, Sillod, Maharashtra, India
[5] Department of Physics, Vivekanand Arts, Sardar Dalipsingh Commerce and Science College, Aurangabad, India
Corresponding Author Email: [1] mspatil9827@gmail.com

Abstract*— We have concentrated on the most current developments in the nanoparticles be from 1 nm up to 100 nm in size; that were widely reported by researchers in the year 2021 in this review. The researchers has used different techniques to create and characterize nanomaterials that could help with unique applications. Scientists have come across numerous societal demands and used scientific and engineering methods to address social issues. Recent advances in science research, agriculture, biotechnology, technology, and medicine have all benefited from the simple to complex structure of nanoparticles. Metal oxide nanoparticles' surface, crystal structure, chemical reactivity, stability, and other physico-chemical properties, among others, are incredibly expressive in determining their functions. These essential properties are influenced by the particle size of the substance. At the nanoscale, the fundamental laws of classical mechanics behave differently, and the material's behaviour can reveal the relationship nature of quantum mechanics.

Index Terms*— Nanoparticles, Nanotechnology, Synthesis methods, Characterization technics.

I. INTRODUCTION

The, is said Greek term "dwarf," which signifies diminutive in size to have been the source of the English word "nano." [1]. The nanoparticles are thought to be the particles identical to biological functional units in size, ranging from ~1 nm to ~100 nm in diameter [2]. They are considered to be recent entrants into the biomedical industry. Nanotechnology investigates structural assessment of electrical, optical, and magnetic activity as well as molecular and sub-molecular levels. It has the potential to change a variety of equipment and procedures used in medicine and biotechnology [3]. These characteristics of magnetic nanoparticles are transportable, less expensive, safer, and simpler to use [3]. The magnetic nanoparticles are better suited for a variety of uses, including biotechnology [4], telecommunication [5], and applications for electrical switching [6], magnetic recording heads [7], antenna rods [8], microwave equipment [9], MLCI [10], resonators [11], and computers and TV equipment [12], pharmaceutical [13], data storage [14], magnetic nanofluid [15], photocatalysis [16], hyperthermia [17]. Memory chip, transformer core, catalyst, magnetic refrigeration, and magnetic resonance imaging are a few examples. Magnetic Nanoparticles are used for a variety of things, including medical treatments, energy storage systems in solar and oxide fuel batteries, optoelectronic devices, bactericidal agents, electronic devices, biological labelling, and the therapeutic interventions of some types of cancer [18-20]. They are also widely incorporated into a variety of standard components such as cosmetics and clothing [21]. Nanoparticles have been receiving a lot of attention recently because to their outstanding qualities, which include antimicrobial activity, great oxidation resistance and a high thermal conductivity [22].

II. SYNTHESIS METHODS

The ceramic method, wet-chemical method, hydrothermal method, spray pyrolysis technique, salt-melt technique, auto-clave method, micro-emulsion method, etc. are some of the good and popular synthesis methods among the diverse portfolio of synthesis methods. Sol-gel auto combustion was employed to create a notional composition of $Ni_{1-x}Cd_xFe_2O_4$ NPs (x = 0.0, 0.2, 0.4). First, a clear, homogeneous solution was made by preserving a 1:3 molar ratio when dissolved nitrates of metal and citric acid in a ratio that was stoichiometric in double-distilled deionized water. Citric acid ($C_6H_8O_7$) is used in wet-chemical procedures more commonly than other fuels because it is a weak organic acid with better complexing properties and a low ignition temperature (200–250 °C). The molecular concentration of metal nitrates to citric acid was thought to be 1:3. The pH of the solution was maintained at 7 by dripping additions of ammonia solution. The mixed nitrate aqueous solution was heated to 80°C and swirled constantly on a magnetic hot-plate stirrer. The hydrolysis of the precursors and the polycondensation of the hydroxide moieties, respectively,

ISSN (Online) 2395-2717

International Journal of Engineering Research in Electrical and Electronic Engineering (IJEREEE)

Vol 10, Issue 1, January 2023

result in the initial creation of "sol" and "gel," which influence the size, shape, porosity, structure, and other physical features of the finished product. This method involved stirring the sol continuously on a magnetic stirrer. The sol was then put into a dish and heated to 80 °C using a hot plate stirrer and heater. The sol was continually stirred for four hours until it solidified as a xerogel. The problem is raised to the next level, and when the temperature reaches 120 °C, self-ignition takes place. The dry gel completely burned after an ignition was started, self-propagating the combustion to produce a fluffy loose powder. The entire auto-combustion process was completed in a short period of time. To create the single-phase $Ni_{1-x}Cd_xFe_2O_4$ ferrite, the as-burnt powder was annealed in the programmed furnace for 6 hours at 600 °C with a heating rate of 10 °C/min.

III. CHARACTERIZATION TECHNIQUES

Using an X-ray diffractometer model (3710) and Cu-Kα radiation (=1.5406 Å), the structural features of the produced $Ni_{1-x}Cd_xFe_2O_4$ (x = 0.0, 0.2, 0.4) nanoparticles were studied.

IV. RESULTS AND DISCUSSION

X-Ray Diffraction Study (XRD)

Using the X-ray diffraction technique, structural analyses $Ni_{1-x}Cd_xFe_2O_4$ was conducted. According to the X-ray study, each sample contains a phase that is FCC, space group $Fd_{\bar{3}m}$ (O_h^7 $No.227$ the spinel structure is nicely matched with JCPDS cards No. 89-4927 and #22-1063. There are no secondary peaks in any of the samples being analyzed, which all have a single phase cubic spinel structure. (see fig. 1). Due to the presence of the matching planes, the XRD pattern shows the creation of a single-phase cubic spinel structure. Table 1 lists the values of structural parameters like peak-to-peak ratios, hopping lengths (L_A, L_B), and bond lengths (R_A, R_B). With an accuracy of ±0.002, the lattice constant (a) of $Ni_{1-x}Cd_xFe_2O_4$ NPs (table 1) was computed [29];

$$a = d\sqrt{(h^2 + k^2 + l^2)} \quad (1)$$

The development of a single-phase cubic spinel structure is demonstrated by the occurrence of the matching planes (220), (311), (222), (400), (422), (511), and (440) in the XRD pattern. The Miller indices are denoted by (h k l), an X-ray wavelength is denoted by (λ), and a glancing angle is denoted by (Θ). The range of the observed lattice constant (a) 8.327, 8.350 and 8.353 Å ±0.002Å. The increase in the lattice constant with the increasing concentration of Cd^{2+} was attributed to the higher ionic radii of Cd ion (0.97 Å); that is greater than the ionic radii of Nickel ion (0.78 Å), and Fe^{3+} (0.645 Å) obeying Vegard's law.

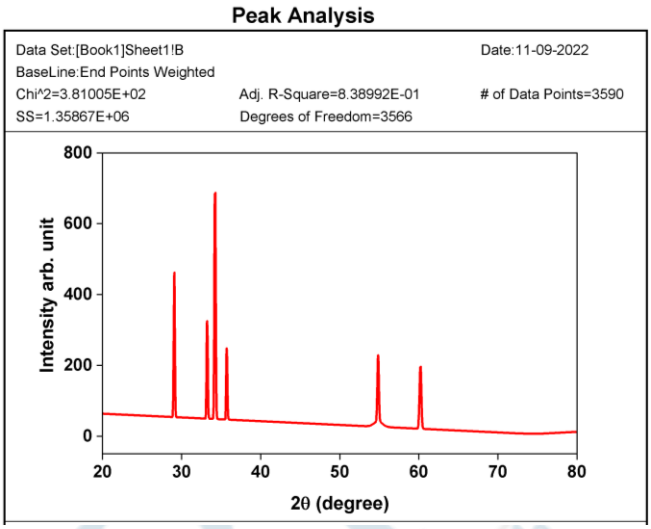

Fig. 1. Typical XRD pattern of $Ni_{1-x}Cd_xFe_2O_4$ nanoparticles for x= 0.2

Table 1. Peak data for the typical sample $Ni_{1-x}Cd_xFe_2O_4$ (x = 0.2)

2Θ	Area Intg	FWHM	Max Height	Area IntgP
29.0922	71.48197	0.16373	410.15303	17.32358
33.25032	50.36154	0.16325	289.81536	12.20506
34.2437	137.13364	0.18305	703.79278	33.23419
35.66761	7.34948	0.08896	78.66962	1.78114
35.74589	30.73339	0.15696	183.94935	7.44821
54.86558	43.48367	0.21422	190.69422	10.53822
54.86558	20.68193	1.2384	15.68915	5.01224
60.21629	51.40255	0.26259	183.90014	12.45735

Table 2. Lattice constant ($a_{Obs.}$) Å, Lattice constant ($a_{Cal.}$) Å, X-ray density (d_x) for $Ni_{1-x}Cd_xFe_2O_4$ (x = 0.0, - 0.4)

Cont. (x)	a(Å) ±0.002Å		X-ray density (d_x)g/cm^3
	$a_{Obs.}$ (Å)	$a_{Cal.}$ (Å)	
0.0	8.327	8.517	5.391
0.2	8.350	8.598	5.593
0.4	8.353	8.680	5.832

The range of the X-ray density was found to be between 5.391, 5.593 and 5.832 Å. Using the Debye-Scherrer formula (2), the size of the crystallite (t) was calculated from the FWHM of the peak having the highest intensity (311) across all reflections [23];

$$t = \frac{0.89\lambda}{\beta cos\theta} \quad (2)$$

Where β = Full Width Half the Maximum of the intense diffracted peak that corresponds to the plane (311) [24], λ = X-ray wavelength; and diffraction angle is θ = 0.89, which is also known as Scherrer's constant. There is a 20–28%

ISSN (Online) 2395-2717

International Journal of Engineering Research in Electrical and Electronic Engineering (IJEREEE)

Vol 10, Issue 1, January 2023

porosity range. Additionally, as Cd content rises, so do the hopping and bond lengths (**table 2**). By comparing the observed intensity ratios with the calculated intensity ratios, the Bertaut technique was utilised to determine the cation distribution as specified in equation (3) using XRD data [25].

$$(Cd^{2+}_{0.4}\ Fe^{3+}_{0.6})^{A}\ [Ni^{2+}_{0.6}\ Fe^{3+}_{1.4}\ ]^{B}\ O^{2-}_{4} \quad (3)$$

Table 3. Composition (x), Tetrahedral bond (d_{AX}) , Octahedral bond (d_{BX}) ,Tetra edges (d_{AXE}), Octa edges (d_{BXE}) for the $Ni_{1-x}Cd_xFe_2O_4$ (x = 0.0, 0.2, 0.4)

x	d_{AX} (Å)	d_{BX} (Å)	d_{AXE} (Å)	Tetra edges	
				Shared d_{BXE}	Unshared d_{BXEU}
0.0	1.889	2.030	3.085	2.802	2.944
0.2	1.893	2.035	3.093	2.810	2.952
0.4	1.894	2.035	3.094	2.810	2.953

V. CONCLUSIONS

A single-phase, cubic shape is produced with the help of solgel method, and spinel lattice structure of ferrite were confirmed by the distinctive XRD responses. With Cd^{2+} loading, it was discovered that the lattice constant (ɑ), X-ray density (d_X), and crystallite size (t) were found to be all increased. The Debye-Scherrer formula being used to determine the crystallite size (t), while the determined lattice constant ranged between 8.327, 8.350 and 8.353 Å ±0.002Å.

REFERENCE

[1] P. Gupta, Introduction and historical background, in: Nanotoxicology in Nanobiomedicine, Springer, 2023, pp. 1-22.

[2] S.S. Mughal, S.M. Hassan, Comparative study of AgO nanoparticles synthesize via biological, chemical and physical methods: a review, American Journal of Materials Synthesis and Processing, 7 (2022) 15-28.

[3] S. Khan, S. Mansoor, Z. Rafi, B. Kumari, A. Shoaib, M. Saeed, S. Alshehri, M.M. Ghoneim, M. Rahamathulla, U. Hani, A review on nanotechnology: Properties, applications, and mechanistic insights of cellular uptake mechanisms, Journal of Molecular Liquids, 348 (2022) 118008.

[4] A.A. Zanker, P. Stargardt, S.C. Kurzbach, C. Turrina, J. Mairhofer, S.P. Schwaminger, S. Berensmeier, Direct capture and selective elution of a secreted polyglutamate-tagged nanobody using bare magnetic nanoparticles, Biotechnology Journal, 17 (2022) 2100577.

[5] J.J. Shea, Magnetic Nanoparticle-Based Hybrid Materials—Fundamentals and Applications, in, IEEE-INST ELECTRICAL ELECTRONICS ENGINEERS INC 445 HOES LANE, PISCATAWAY, NJ …, 2022.

[6] M. Karpets, M. Rajnak, V. Petrenko, I. Gapon, M. Avdeev, L. Bulavin, M. Timko, P. Kopcanský, Electric field-induced assembly of magnetic nanoparticles from dielectric ferrofluids on planar interface, Journal of Molecular Liquids, 362 (2022) 119773.

[7] G. Vijayasri, R.C. Bhaskar, J. Rajesh, An essential advancement of magnetic nanoparticles, in: Fundamentals and Industrial Applications of Magnetic Nanoparticles, Elsevier, 2022, pp. 41-63.

[8] K.N. Pawar, A.A. Nawpute, S. Tambe, P. Patil, Y. Ubale, A. Patil, Dextrose Assisted Sol-Gel Synthesis and Evaluation of Structural Parameters of Li0. 5Fe2. 5O4 Nanoparticles for Microwave Device Application, in: Advanced Materials Research, Trans Tech Publ, 2022, pp. 27-33.

[9] H.-s. Li, A.-m. Wu, T. Cao, H. Huang, The absorption mechanism for magnetic waves and research progress on carbon-coated magnetic nanoparticles, New Carbon Materials, 37 (2022) 695-706.

[10] S.R. Daf, D.S. Badwaik, S.M. Suryawanshi, V.S. Harode, B.R. Balbudhe, Physical, spectroscopic and antibacterial investigation of Mg0. 3Zn0. 5Mn0. 2Fe2O4 via temperature dependent hydrothermal approach, Journal of Magnetism and Magnetic Materials, 567 (2023) 170346.

[11] Y. Malallah, K. Alhassoon, G. Bhuta, A.S. Daryoush, RF Characterization of 3-D-Printed Tunable Resonators on a Composite Substrate Infused with Magnetic Nanoparticles, IEEE Microwave and Wireless Components Letters, 32 (2022) 1175-1178.

[12] A. Iqbal, M.R. Jan, J. Shah, M.N. Sarwar, Removal of Cu (II) from acid leach solution of electronic waste utilizing magnetic activated carbon derivatized with α-benzoinoxime: Alternate mining source, Journal of Chemical Technology & Biotechnology.

[13] M.M. Bhatti, S.M. Sait, R. Ellahi, Magnetic nanoparticles for drug delivery through tapered stenosed artery with blood based non-newtonian fluid, Pharmaceuticals, 15 (2022) 1352.

[14] B. Garcia-Merino, E. Bringas, I. Ortiz, Synthesis and applications of surface-modified magnetic nanoparticles: Progress and future prospects, Reviews in Chemical Engineering, 38 (2022) 821-842.

[15] J. Philip, Magnetic nanofluids: Recent advances, applications, challenges, and future directions, Advances in Colloid and Interface Science, (2022) 102810.

[16] N. AbouSeada, M. Ahmed, M.G. Elmahgary, Synthesis and characterization of novel magnetic nanoparticles for photocatalytic degradation of indigo carmine dye, Materials Science for Energy Technologies, 5 (2022) 116-124.

[17] C. de la Encarnación, D.J. de Aberasturi, L.M. Liz-Marzán, Multifunctional plasmonic-magnetic nanoparticles for bioimaging and hyperthermia, Advanced Drug Delivery Reviews, (2022) 114484.

[18] P. Gupta, Nanotoxicology in Nanobiomedicine, Springer Nature, 2023.

[19] K. Aimonen, E. Ekokoski, U. Forsström, S. Hemming, R. Joro, H. Kangas, S. Kauppi, P. Kautto, P. Koivisto, M. Korkalainen, Nanomaterials as part of society: Towards a safe future of nanotechnology, (2022).

[20] D. Song, X. Chen, M. Wang, X. Xiao, Sensors International.

[21] S.A. Al-Sayed, M.O. Amin, E. Al-Hetlani, Magnetic Nanoparticle-Based Surface-Assisted Laser Desorption/Ionization Mass Spectrometry for Cosmetics Detection in Contaminated Fingermarks: Magnetic Recovery and Surface Roughness, ACS omega, 7 (2022) 43894-43903.

[22] R. Jiang, X. Zheng, S. Zhu, W. Li, H. Zhang, Z. Liu, X. Zhou, Recent Advances in Functional Polyurethane Chemistry: From Structural Design to Applications, ChemistrySelect, 8

(2023) e202204132.

[23] S.K. Sen, U.C. Barman, M. Manir, P. Mondal, S. Dutta, M. Paul, M. Chowdhury, M. Hakim, X-ray peak profile analysis of pure and Dy-doped α-MoO3 nanobelts using Debye-Scherrer, Williamson-Hall and Halder-Wagner methods, Advances in Natural Sciences: Nanoscience and Nanotechnology, 11 (2020) 025004.

[24] S. Talam, S.R. Karumuri, N. Gunnam, Synthesis, characterization, and spectroscopic properties of ZnO nanoparticles, International Scholarly Research Notices, 2012 (2012).

[25] P. Belavi, G. Chavan, L. Naik, R. Somashekar, R. Kotnala, Structural, electrical and magnetic properties of cadmium substituted nickel–copper ferrites, Materials Chemistry and Physics, 132 (2012) 138-144.